*Geophysical Research Letters*

Supporting Information for

# Relaxation of wind stress drives the abrupt onset of biological carbon uptake in the Kerguelen Bloom: a multisensor approach.

**Violaine Pellichero[1], Jacqueline Boutin[1], Hervé Claustre[2], Liliane Merlivat[1], Jean-Baptiste Sallée[1], and Stéphane Blain[3]**

[1]Sorbonne Université, CNRS, IRD, MNHN, UMR 7159, Laboratoire d'Océanographie et du Climat : Expérimentations et Approches Numériques, LOCEAN-IPSL F-75005, Paris, France

[2] Sorbonne Université, CNRS, UMR 7093, Laboratoire d'Océanographie de Villefranche, LOV, 06230 Villefranche sur Mer, France

[3]Sorbonne Université, CNRS, UMR 7621, Laboratoire d'Océanographie MICrobienne, LOMIC, F-66650, Banyuls sur Mer, France

## Contents of this file

Text S1 to S7
Figures S1 to S7

## Introduction

**In this Supplementary Information section, we introduce several figures as well as additional information in support of the main text. We give details on the methods used to estimate the mixed-layer depth based on the mooring data in one hand, and on the BGC-Argo floats in another hand. Moreover, we introduce the detailed decomposition of the net heat fluxes estimated from 4 different products and assess the wind contribution to the stratification of the water column. We also introduce additional information about the WMO 6902736 BGC-Argo float that are not shown in the main text. We fully describe the method to estimate the NCP based on DIC evolution. The dynamics of the phytoplankton bloom as observed on the BGC-Argo float data and on the mooring data is compared. This step allows us to be confident in considering the bloom development as a regional signal of the onset and not only as an advected patch of phytoplankton. Finally, we further investigate the vertical**

**structure of the surface layer to distinguish different dynamic within the mixing and mixed-layer.**

**Text S1. Testing the Mixed-layer Depth Calculation from Different Methods**

The ocean mixed-layer is commonly defined as the ocean surface layer in which physical properties such as temperature, salinity, and density are well mixed, i.e., nearly homogeneous with depth. The mixed-layer depth (MLD) has become a reference concept in oceanography because it plays the essential role of intermediary between the atmosphere and the deep ocean. A number of criteria have been developed over the years to compute MLD based on a given density, salinity, or temperature profiles (de Boyer Montégut et al., 2004; Holte & Talley, 2009).

The most widespread method for finding the MLD is the threshold method which search for the depth at which the temperature or density profiles change by a predefined amount relative to the surface reference value. Moreover, it has been shown that methods working on density profiles rather than temperature profiles are more successful in detecting the base of the MLD (Sallée et al., 2006; Pellichero et al., 2017). Based on such studies, we performed numerous tests in order to find the best MLD estimate from our data. Our methods of MLD computation are all based on individual profiles from BGC-Argo floats and mooring.

First, we compute the MLD with a density threshold criterion of $\Delta\sigma = 0.03$ kg $m^{-3}$ as shown in Figure. S1a. In black are plotted the two MLD from the two BGC-Argo floats (WMO 6902737 in dashed black line and WMO 6902736 in black line), and in red is the MLD estimated from the mooring which means this MLD is estimated only from the SBE-37 sensors since they are the only ones that can provide salinity estimate and thus the density. This result shows that the different MLD are consistent with each other and there is a good correspondence between floats and mooring which gives us confidence in our MLD estimate.

The calculation of the MLD is therefore equivalent according to the data (mooring or BGC- Argo floats), but this is also true according to the detection methods used. Indeed, in Figure. S1b we also compared the density threshold method (dashed black line) with the temperature threshold method (black line) for WMO 6902737 float. Here we use a temperature criterion for the detection of the base of the MLD about $\Delta T = 0.2$ °C $m^{-1}$. Once again, the two methods are nearly the same. Following these tests, we decided to work only with the temperature threshold method in order to use both SBE-37 and SBE-56 mooring sensors and thus to improve the vertical resolution of the MLD at the mooring.

Moreover, we remark in some points in Figure. S1a that the MLD estimate from the BGC-Argo floats are shallower than those from the mooring. Therefore, we wondered if the absence of data above 42 m may introduce errors in our estimation of the MLD from the mooring. To tackle this question, we remove the data of the floats above 42 m and we redo the same calculation of MLD. The result is introduced in Figure. S1c where we can see the dashed black line which is the MLD estimate (from temperature threshold method) from WMO 6902736 without any data above 42 m. Indeed, we notice that the MLD without surface data is this time slightly deeper than the origin (black line) and is

getting closer to the MLD from the mooring (red line). This result suggests that sometimes the MLD from the mooring overestimates the MLD, but it occurs on rare occasions and practically not during the studied period of the onset of the phytoplankton bloom i.e. before November 05, 2016.

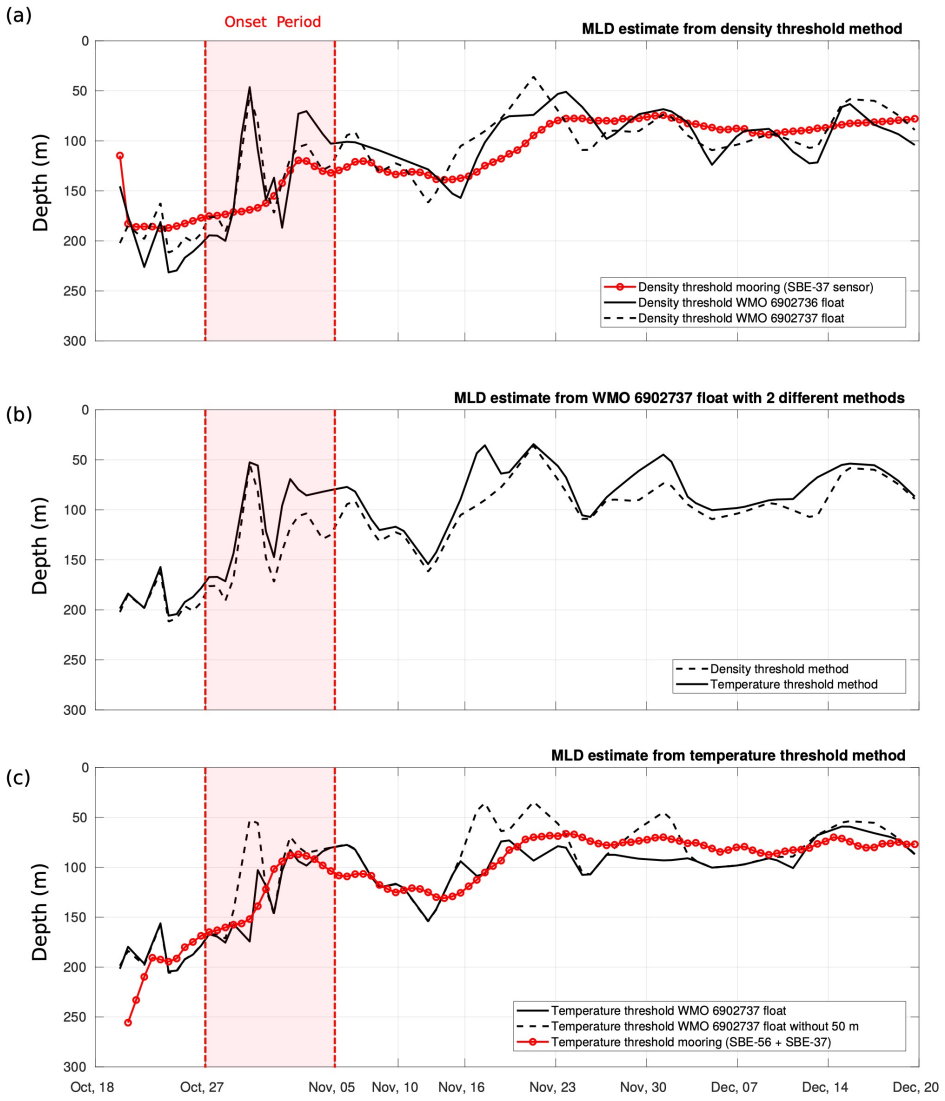


**Figure S1.** Mixed-layer depth estimates (in m) from different methods. (a) Time series of the MLD estimated from the density threshold method ($\Delta\sigma$= 0.03 kg $m^{-3}$). The black lines are the MLD based on BGC-Argo floats and the red line is the MLD from the mooring (i.e. using only SBE-37 sensors that record the conductivity and allow to estimate the density). (b) Comparison between the MLD given by the density threshold method (dashed black line) and the temperature threshold method (black line, $\Delta T$ = 0.2 °C $m^{-1}$) for the WMO 6902737 float. (c) Time series of the MLD presented in the main text and

estimated from the temperature threshold method based on the mooring (red line), the WMO 6902737 float (black line) and the WMO 6902737 float where we previously removed the data between 42 m up to the surface (dashed black line).

## Text S2. Relative Contributions to Heat Fluxes versus Wind

The net heat flux shown in Figure. 2c is the sum of four contributions: latent flux (top right panel), sensible flux (top left panel), short wave (bottom left) and longwave (bottom right). All the 4 products used give consistent results and show that the net heat flux was stabilizing the water column (positive values) since at least September 2016.

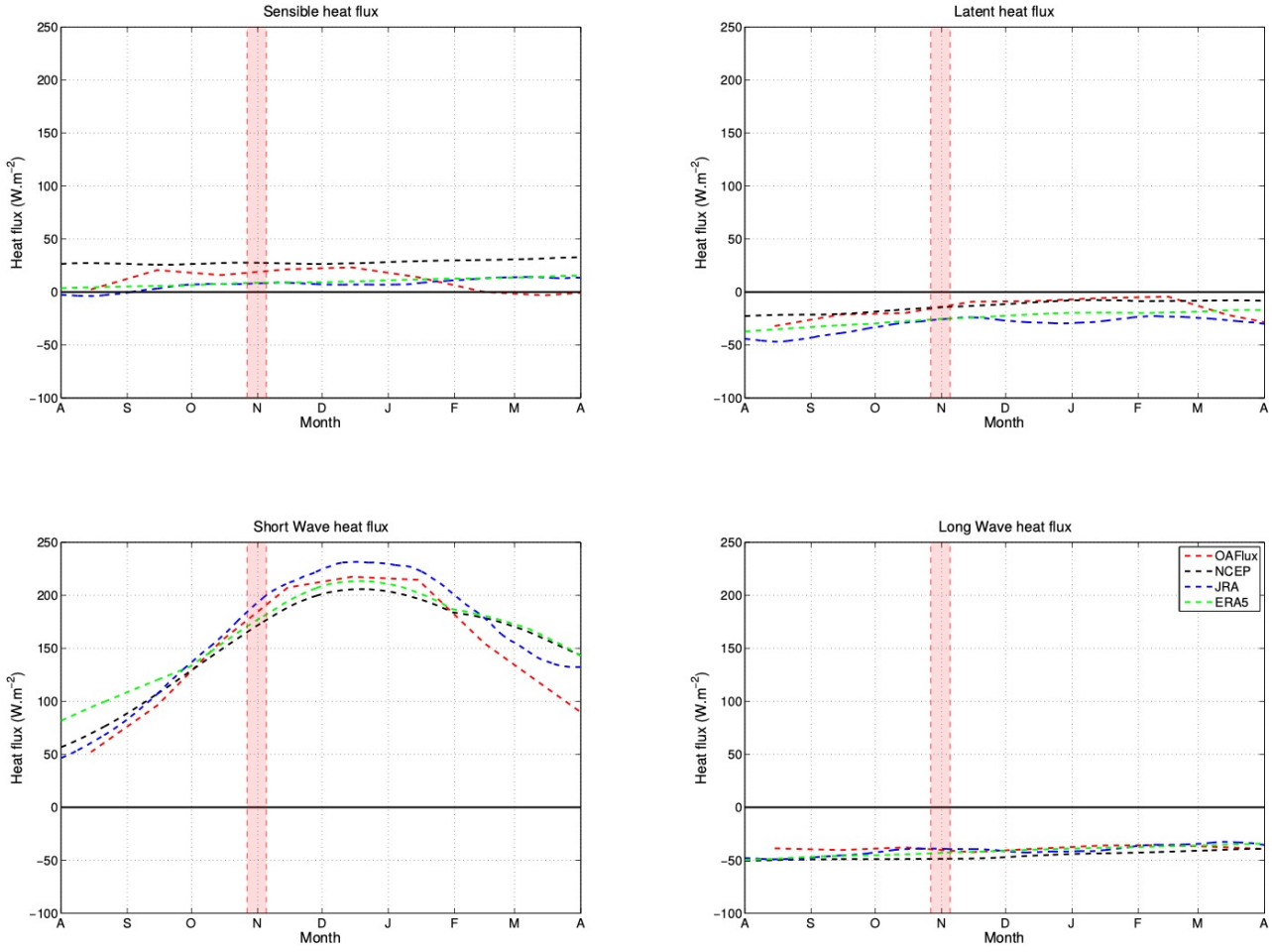


**Figure S2. Decomposition of the net heat flux into sensible heat flux (top right), latent heat flux (top left), shortwave (bottom left) and longwave (bottom right).** Each component of the heat flux is shown for the 4 products used in this study from August

2016 to April 2017 (OAFlux in red, NCEP1 in black, JRA-55 in blue and ERA5 in green). The red shading indicates the onset period of the bloom (27 Oct to 5 Nov, 2016).

As the water column stratifies from at least September 2016, we investigated the wind stress (Figure. 2d) in order to explain how we can observe a rapid stratification of the MLD associated to the bloom at the end of October. Theoretical works indicates that when acting on a stratified fluid, the typical length scale where wind mixing acts, the "mixing-layer", is the Ozmidov length ($L_{OZ}$) defined as (Denman and Gargett, 1983; Riley and Lelong, 2000; Brody and Lozier, 2015):

$$L_{OZ} = (2\pi)\varepsilon^{1/2}N^{-3/2} \qquad \text{(A1)}$$

Where N is the frequency of Brunt-Väisälä defined as $\mathrm{N}^2 = -\frac{g}{\rho}\frac{\partial \rho}{\partial z}$ and ε is the rate of turbulent kinetic energy dissipation equal to $w_*^3/\kappa z$ at depth $z = 42\,m$, with $w_*$ the friction velocity and κ the Von Kármán constant. The friction velocity at the mooring site is estimated from the wind-stress output of several different atmospheric reanalysis: $w_* = \sqrt{\tau/\rho}$, where $\tau$ is the wind-stress, and $\rho$ is the sea-water density. At the mooring site we estimate N from its temperature contribution: $\mathrm{N}^2 = -\alpha g\frac{\partial T}{\partial z}$, where $\alpha$ is the thermal contraction coefficient, and T is the water-column temperature estimated from the mooring temperature sensors. The gradient of temperature is estimated between 42 m and the base of the mixed-layer.

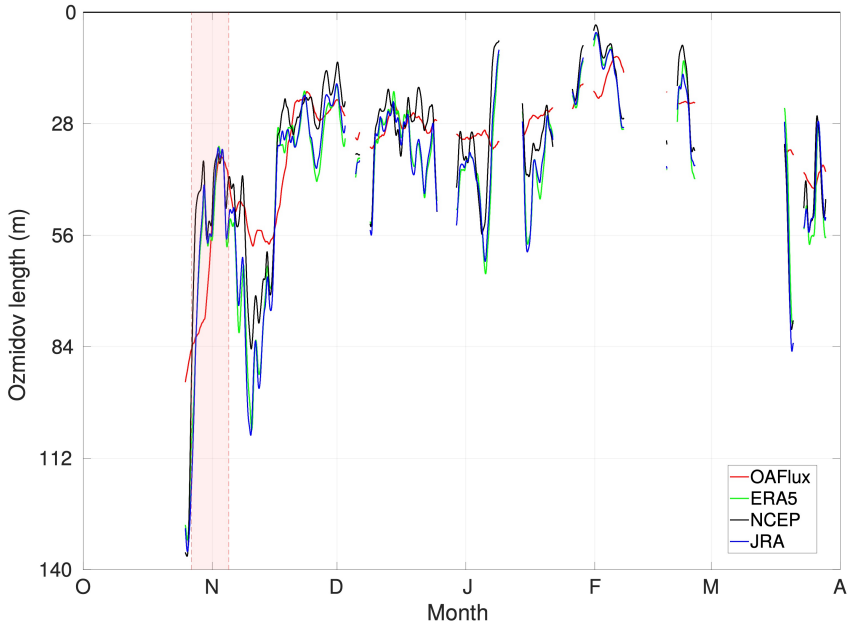


**Figure S3. Mixing-layer estimated from the 4 products of wind stress used in this study** (OAFlux in red, NCEP1 in black, JRA-55 in blue and ERA5 in green). The red shading indicates the onset period of the bloom (Oct 27 to Nov 05, 2016)

The Figure. S3 showing the mixing-layer estimated from the 4 products, indicates that before the beginning of the bloom, the wind even if decreasing (Figure. 2d) was strong enough to mix the upper 130 m (according to NCEP1, ERA5 and JRA) and then balanced the stratifying effect of the heat flux. Then, right at the October 27, the mixing length reduces to 40-50 m as wind stress is still decreasing allowing the MLD to shoal, the vertical stratification to enhance and the bloom to initiate.

**Text S3. Data from the WMO 6902736 float**

Two BGC-Argo floats were deployed during the SOCLIM voyage. In this section we present the data from the WMO 6902736 BGC-Argo float. As mentioned in the main text, both results are very similar. As in Figure. 3d, we notice a large increase of the Chla during the onset period (27 Oct. to 05 Nov.).

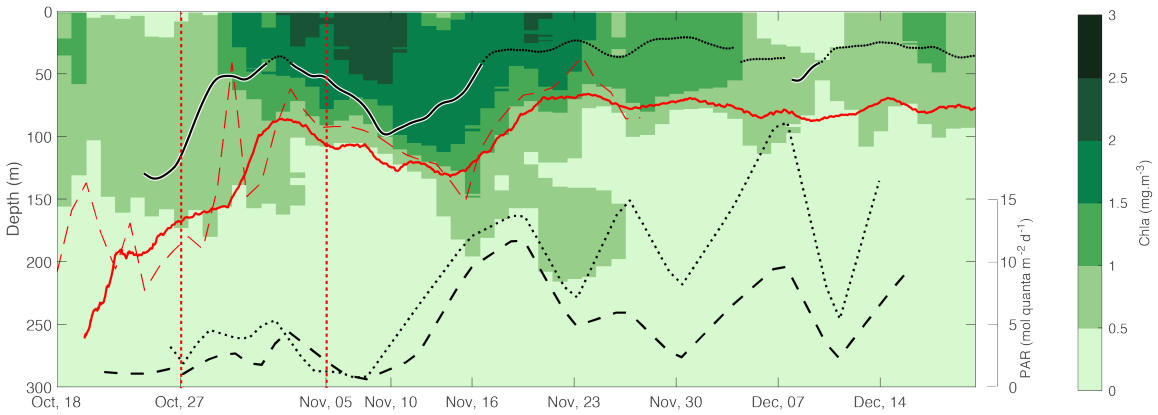


**Figure. S4.** Vertical section of Chla (WMO 6902736 BGC-Argo float); MLD and mixing-layer computed at the mooring site are shown as plain red and black lines respectively, and MLD from the float time-series is shown as red dashed line for comparison; $PAR_{MLD}$ and $PAR_{MixLD}$ are shown as black dashed and dotted lines, respectively. The onset period of the bloom (October 27, 2016 to November 05, 2016) when DIC decreased linearly versus time (see Figure. 3b) is shown as the two vertical red dashed lines.

**Text S4. Eulerian VERSUS Lagrangian View: Comparison of the Dynamics of the Bloom from the Mooring and from the BGC-Argo Float**

The mooring is the Eulerian way to study the ocean as it is stationary at a fixed location. This has some implications for the results in terms of water mass advection for example. Indeed, when analyzing the onset of the phytoplankton bloom from mooring data, how to make sure that the mooring does not sample an advected water mass? One way to answer this question is to compare the dynamics of the phytoplankton bloom at the mooring point and the dynamics of the phytoplankton bloom seen by the BGC-Argo floats which provide Lagrangian measurements.

The Figure. S5 introduces such a comparison with the dynamics of the phytoplankton bloom seen by the mooring in black line and that record by the WMO 6902737 float in red and WMO 6902736 in blue. In order to observe the same quantities, and knowing that the mooring fluorimeter is fixed at 42 m depth, we look at the Chla concentration at 42 m for the BGC-Argo floats. Two main differences remain between the mooring and the BGC-Argo floats: (1) the fluorimeter saturation level is at 5 mg $m^{-3}$, which means that the Chla from the mooring may be higher, and (2) the values from the mooring are ~2.5 times higher than those record by the BGC-Argo floats partly due to different fluorometers on the mooring and the BGC-Argo floats leading to difference of calibration (Roesler et al., 2017). Despite the differences limiting the analyse to relative variations rather than absolute values of Chla, the dynamics of the bloom development (the red area) recorded both from the mooring and the BGC-Argo floats is essentially identical with a sharp increase at the same period. This result indicates that what the mooring records in one location is not an advected patch of phytoplankton, but it is well representative of a regional signal of the onset of the bloom.

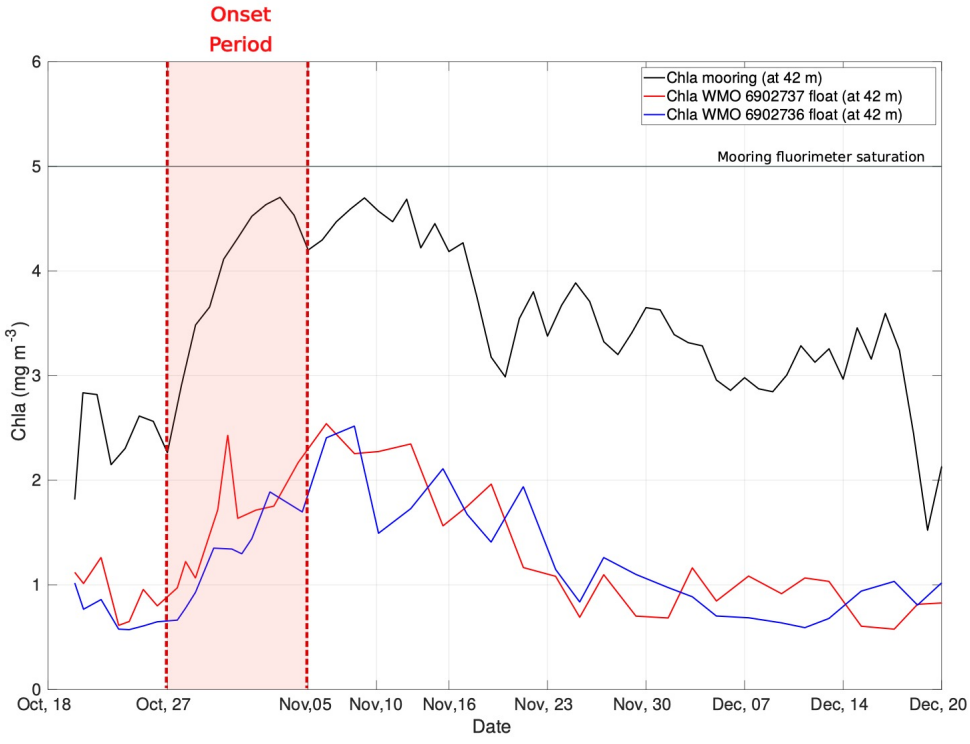


**Figure S5.** Time series of the Chla concentration in mg $m^{-3}$. Comparison between the dynamics of the bloom recorded by the mooring at 42 m depth in black line and that recorded by the WMO 6902737 (red) and WMO 6902736 (blue) floats also at 42 m

depth in red line. The horizontal line corresponds to the level of saturation of the mooring fluorimeter which is at 5 mg $m^{-3}$.

## Text S5. Quantitative Estimate of in-situ Net Community Production (NCP)

**Calculation of DIC and Alkalinity:** Dissolved inorganic carbon, DIC (µmol $kg^{-1}$), is derived from $pCO_2$, alkalinity, temperature and salinity using the $CO_2$ dissociation constants of Mehrbach et al. (1973) as refitted by Dickson and Millero (1987). Alkalinity (Alk), is computed from salinity (Sal) using the alkalinity-salinity relationship (Figure. S6) derived from samples collected at a nearby location, station A3 (OISO cruise):

$$Alk = 58.17\ Sal + 313.55 \quad (r^2 = 0.94)$$

where Alk is expressed in µmol $kg^{-1}$. The relative precision of successive DIC values is expected to be 0.5 µmol $kg^{-1}$ (Merlivat et al, 2015).

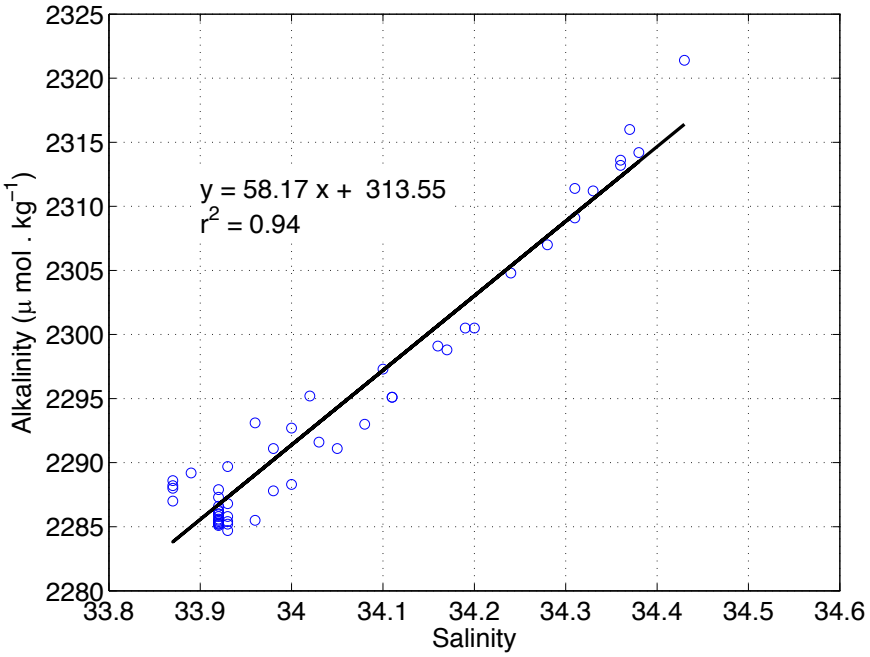


**Figure S6**. Relationship between alkalinity and salinity derived from the OISO cruises on October 2016 and January 2017 at the station A3. Solid line is linear fit through the data.

**Calculation of the air-sea $CO_2$ flux:** we estimated the air-sea $CO_2$ flux of 10.8 mmol $m^{-2}$ $d^{-1}$ with the following equation:

$$\left(\frac{\Delta DIC}{\Delta t}\right)_{air-sea} = k.s\left(pCO_{2atm} - pCO_{2sea}\right) \qquad (A2)$$

Where k is the gas transfer velocity (Wanninkhof, 2014), s is the solubility of $CO_2$ and $pCO_{2sea}$ and $pCO_{2atm}$ are respectively the partial pressures of $CO_2$ in the water and in the above lying air.

**Influence of eddy diffusion and of integration depth:** We perform sensitivity test where we integrate NCP over the mixed-layer depth assuming a homogeneous vertical DIC profile over the mixed-layer instead of over the mixing-layer depth and where we additionally take into account a vertical eddy diffusion term as follows:

$$NCP = \left(\frac{\Delta DIC_{int}}{\Delta t}\right)_{bio} = \left(\frac{\Delta DIC_{int}}{\Delta t}\right)_{meas} - k \times s \times (pCO_{2atm} - pCO_{2sw}) - K_z \times \frac{dDIC}{dz} \quad \text{(A2)}$$

The eddy diffusion term, is estimated to be 7.8 mmol $m^{-2}$ $d^{-1}$ (i.e. less than 4 % of the NCP) using a spatially constant vertical diffusion coefficient of $K_z = 3.10^{-4}$ $m^2 s^{-1}$ (Park et al., 2008) and the vertical gradient of DIC recorded at the basis of the mixed-layer during the OISO cruise on the 18th and 24th October, 2016 (dDIC/dz = 0.3 µmol $kg^{-1}m^{-1}$). Hence it is negligible in front of the NCP integrated in the mixed-layer (212 mmol $m^{-2}$ $d^{-1}$). Since we expect the DIC gradient at the basis of the mixing-layer to be less than the one at the basis of the mixed-layer, the influence of the eddy diffusion term on the estimate of NCP integrated over the mixing-layer is expected to be less than 7.8 mmol. $m^{-2}d^{-1}$, i.e. an uncertainty less than 7%.

**Text S6: Chla climatology computation**

We used a climatology of satellite Chla data processed and distributed by ACRI-ST GlobColour service (http://marine.copernicus.eu) to describe the seasonal cycle of Chla averaged at the mooring site. The climatology (1998-2017) is created using data falling into a moving temporal window of ± 5 days (i.e. 11 days).

**Text S7: Chla in MLD and mixing-layer**

In this section, we look at specific Chla profiles to convince ourself that there is indeed a different dynamic within the mixing and mixed-layer. It is clear both on the vertical section (upper panel, Figure. S7) and even more obviously on a set of individual profiles (lower panel, Figure. S7), that there is a two-layer structure within the MLD. While the upper 50 meters or so are associated with high Chla concentration, the lower part of the MLD have much weaker Chla concentration. This structure within the MLD is very suggestive that the MLD is not actively mixed during this time. Now, plotting the estimated mixing-layer depth, it shows clearly that the high Chla concentration in the upper part of the MLD is within the mixing-layer (Figure. S7b). The estimated mixing-layer depth predicts impressively well the vertical boundary, within the MLD, separating high Chla concentration in the upper part of the MLD, with sharp decrease with depth of Chla concentration in the lower part of the MLD.

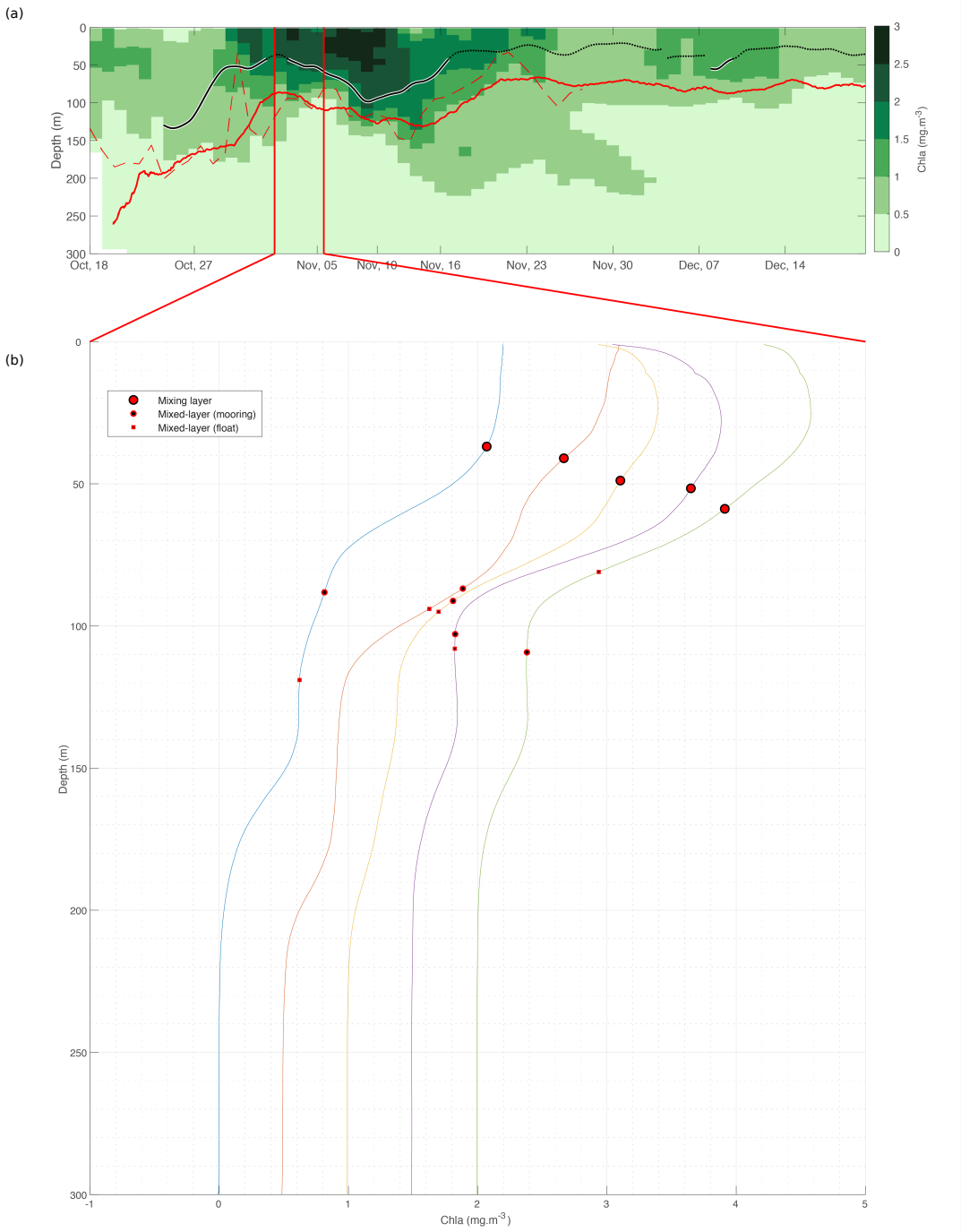


**Figure S7**. (a) Same as Figure. 3d (WMO 6902737 BGC-Argo float). (b) A set of individual Chla profiles with mixed-layer depths estimates from the mooring (black circle), from the BGC-Argo float (black square) and mixing-layer depths (red circle).